Large Deformation Modelling of Tight Woven Fabric under High Air Pressure

Xueliang Xiao, Andrew Long, Hua Lin, Xuesen Zeng

The University of Nottingham, Nottingham, Nottinghamshire UNITED KINGDOM

Correspondence to:
Xueliang Xiao email: xiao_xueliang@163.com

ABSTRACT

Technical textiles used in airbag are usually in tight structure and subject to high air pressure in through-thickness direction. The pressure can deform fabric with changing its properties such as porosity and air permeability. This paper proposes an analytical approach to predict the out-of-plane deformation of tight fabric by analogy with membrane deformation. The model integrates the energies happened on the deformed fabric, that is, fabric strain energy, bending energy, and external work done. The fabric deformation can be predicted by minimizing the total fabric energy. The prediction was validated by experiment for fabric profile and the maximum displacement, and a good agreement was found for the cases of two typical fabrics. A sensitivity study shows that Young's modulus and Poisson's ratio can affect the fabric deformation significantly.

INTRODUCTION

Whether a woven fabric is under an out-of-plane constant pressure or transient impact, it is important to understand its deformation mechanism since the deformation can alter the fabric structure and the following air permeability, such as airbag fabric deformation under more than 2 *bar* pressure when inflation. The low permeability of tight airbag fabric may thereafter have a longer period of effective protection under the deformation. Thus, this paper desires to predict the tight fabric deformation with two investigable terms, the maximum displacement and the fabric profile of deflection [1, 2].

As is known, a few mechanical manners of textiles are usually nonlinear. For example, the fabric load-extension curves from uniaxial or biaxial tensile tests are never straight lines. This non-linearity is primarily caused by the weave structure and the crimped fibers in yarns as reported by Clulow and Taylor [3]. More precisely, the tensile non-linearity also depends on the fiber itself like its crimpness, fineness, stiffness, and friction. Experimentally, Kawabata studied the relationship and developed an evaluation system (KES), which can measure the fabric uniaxial, biaxial and shear deformations, and the KES theoretical basis [4-6] which assumes both warp and weft yarns perfectly flexible. Other analytical models were also developed to predict the fabric stress-strain curves [7, 8] and to be verified by KES (KES-FB1) [7]. In solid mechanics, the slope of stress-strain curve equals Young's modulus (E), which is determined by the compositions and structure of fabric [5, 6]. Poisson's ratio (ν) is another physical factor relating to the stress-strain non- linearity in the fabric deformation. The ν first increases towards a maximum value due to the rapid shrinkage of the sample in the transverse direction, and then decreases when the yarn crimps are exhausted [9]. Lu [10] developed a method to determine the ν value of woven fabric based on a biaxial extension and suggested the value in the range of 0 to 0.5. Hursa [11] measured the ν value of woven fabric with digital image correlation based on the standard ISO 13934-1:1999. The fabrics were exposed to a 1% strain rate on a tensile test machine. Testing was simultaneous with recording using a digital video camera. The video recordings were afterwards processed in a MATLAB program and the ν values were determined according to the ratio of strains in x and y axis directions. The results showed the ν values of fabrics were in the range of 0.2 and 0.5 for warp and weft directions.

The fabric deformation under high air pressure is similar to fabric draping, where a fabric is forced over a fixed mould. Wang [12] utilized a pin-jointed net model to evaluate the yarn slippage in fabric draping. The results showed the slippage can be ignored in the fabric out-of-plane deformation. This model [12,13] was found to be a good way to interpret the fabric deformation mechanism.

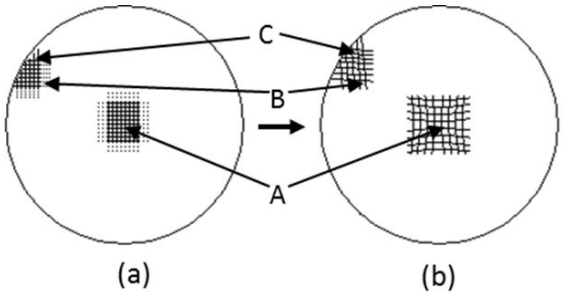

FIGURE 1. The pin-jointed net model for circular clamped fabric: (a) flat sheet; (b) deformed sheet.

Figure 1 shows the predominant deformation areas of a circular fabric. The central part 'A' mainly has tension and compression effects, the area 'B' exhibits shear and tension effects while the area 'C' exhibits bending, shear and extension effects [14, 15]. Tensile and shear deformation of yarns take place in the fabric planar, and undertake the majority of external loading. Hu [15] simulated the draping of a circular fabric sheet, showing draping is a typically large displacement deformation like buckling. The maximum displacement is much larger than the fabric thickness. The mid-plane stretches and hence the in-planar tension increases within the sheet and causes a considerable load resistance. This cannot be predicted by the small-deflection theory. For such a situation, the large sheet deformation can be employed to evaluate the fabric deformation if the fabric can be approximated as a thin sheet. The large deformation theory assumes that the deflections are no longer small in comparison with the thickness but are nevertheless small compared with the remaining sheet dimensions.

Mathematical formulas can be used to describe the deformed fabric configuration. For example, Ugural [16] reported a set of expressions for the maximum deflection (w') of a clamped circular plate (radius a) subjected to a uniform load as shown in *Figure 2*:

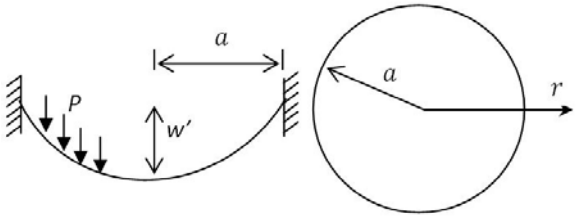

FIGURE 2. A clamped circular plate deformed by a uniform loading [16].

The displacement of any point on the deformed plate in in-planar and out-of-plane are assumed:

$$w = w'(1 - \frac{r^2}{a^2})^2 \quad (1a)$$

$$u = r(a - r)(c_1 + c_2 r) \quad (1b)$$

where u and w are the displacements in in-planar and out-of-plane directions, w' is the maximum displacement, r is the radial position, c_1 and c_2 are factors depending on the boundary conditions. Eq. (1) is suitable for a continuous and rigid sheet. The factors in the assumptions should be derived for the deformed configuration.

Lin [17] modelled the deformation of a textile sheet caused by its own weight, assuming an initially flat, stress-free square material sample of length Eq. (2b).

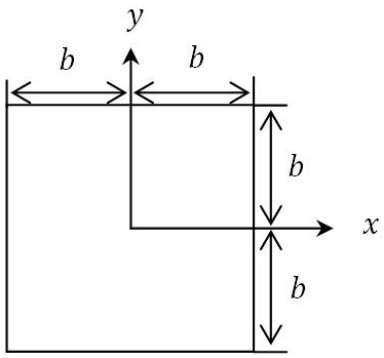

FIGURE 3. The geometry and co-ordinate axes for the draping of a square sheet [17].

The clamped sheet deforms into a curved shape under gravity. *Figure 3* shows the geometry and the co-ordinate axes for the problem. The following approximations were assumed for the displacements in three dimensions:

$$u = cx(\sin(\frac{\pi x}{b}) + \cos(\frac{\pi y}{2b})) \quad (2a)$$

$$v = cy(\sin(\frac{\pi y}{b}) + \cos(\frac{\pi x}{2b})) \quad (2b)$$

$$w = w'(\frac{1}{2}\cos(\frac{\pi x}{2b}) + \frac{1}{2}\cos(\frac{\pi y}{2b})) \quad (2c)$$

where c is an unknown factor. Eq. (2) assumes the displacements only for a square woven fabric under a uniform load (or gravity) but the results showed a good agreement between prediction and simulation.

Inspired from the above review, this paper models the out-of-plane deformation of a clamped circular fabric under high air pressure. Expressions are also postulated for the deflection by considering appropriate boundary conditions. The Timoshenko large deflection sheet theory [18] is employed for analysing the deformation since this theory is frequently encountered in the investigation of large deflection of thin plates [17, 19, 20]. The advantage of the energy-based model is that it incorporates the material nonlinearity and geometric nonlinearities, which are characteristics of fabric mechanical issues.

ANALYTICAL MODELING

The fabric deformation under high air pressure is modelled in macro-scale (the fabric dimension is at least 100 times greater than its yarn dimension) by considering an originally flat, stress-free circular tight fabric in deformation. The tight fabric has so large fiber volume fraction that it can be assumed as a thin membrane, and its out-of-plane deflection is assumed to be approximately axisymmetric without yarn slippage due to the compaction of yarn crossover by the high air pressure and yarn tensioning. Cylindrical coordinates are used in this particular deflection situation.

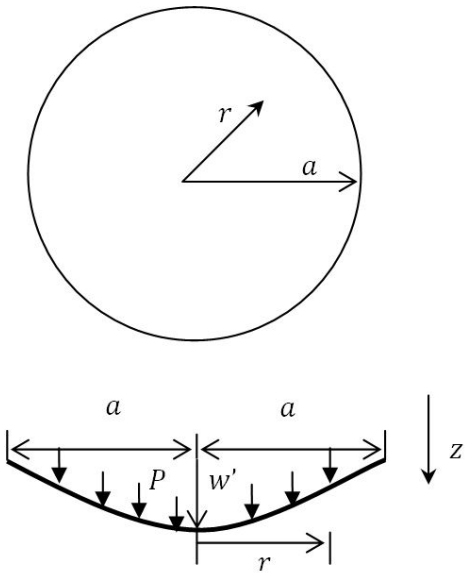

FIGURE 4. Schematic of geometry and polar coordinates for a deformed circular fabric.

Figure 4 shows a clamped circular fabric from top view and its deflection profile under pressure *P* by side view. The origin of cylindrical coordinates is placed at the centre of the fabric. The fabric edge is clamped by two annular plates, giving the fabric radius a. The in-plane and out-of-plane directions are represented as r and z. The boundary conditions are found as:

$$r = 0, u = 0; r = a, u = 0; \tag{3a}$$

$$r = 0, w = w', \frac{dw}{dr} = 0; r = a, w = 0; \tag{3b}$$

where u and w are the displacements in r and z direction, respectively; w' is the maximum displacement in z direction.

Owing to the axisymmetric geometry and the uniform distributed pressure, it can be inferred that w is an even function of r whereas u is an odd function of r.The requirements can be satisfied by taking the following trigonometric approximations for the displacements in two directions:

$$u = \varphi * \sin(\frac{\pi r}{a}) \tag{4a}$$

$$w = w' \cos(\frac{\pi r}{2a}) \tag{4b}$$

where φ is an arbitrary constant. It is noted that the shape of Eq. (4) is different from the reviewed approximation of Eq. (1) that Eq. (4) exhibits less gradual deflection near the edge of clamped area. The problem of determining the fabric deflection reduces to the derivation of the coefficients φ and w' in Eq. (4). The coefficients can be determined by the principle of virtual displacements. Three types of energy take place during the deflection: bending energyU_b, fabric strain energy U_m and work done U_w by air pressure.

Firstly, bending energy (U_b) is defined in polar coordinates as:

$$U_b = \frac{D}{2}\iint_0^A \{\left(\frac{\partial^2 w}{\partial r^2} + \frac{1}{r}\frac{\partial w}{\partial r} + \frac{1}{r^2}\frac{\partial^2 w}{\partial \theta^2}\right)^2 - 2(1-\nu)\frac{\partial^2 w}{\partial r^2}\left(\frac{1}{r}\frac{\partial w}{\partial r} + \frac{1}{r^2}\frac{\partial^2 w}{\partial \theta^2}\right) + 2(1-\nu)\left(\frac{1}{r}\frac{\partial^2 w}{\partial r \partial \theta} - \frac{1}{r^2}\frac{\partial w}{\partial \theta}\right)^2\} r dr d\theta \tag{5}$$

where A is the area of the fabric surface, ν is the fabric Poisson's ratio. Eq. (5) is important for a rigid sheet, however, herein has little contribution to the total deformation energy due to the fabric flexibility. Eq. (5) can be reduced to a concise form of Eq. (6) due to the axisymmetric bending of the deformed fabric:

$$U_b = \pi D \int_0^a \{\left(\frac{\partial^2 w}{\partial r^2} + \frac{1}{r}\frac{\partial w}{\partial r}\right)^2 - \frac{2(1-\nu)}{r}\frac{dw}{dr}\frac{\partial^2 w}{\partial r^2}\} r dr \tag{6}$$

where $\mathbb{D}$ is the fabric flexural rigidity, which does not equal $\frac{EL^3}{12(1-\nu^2)}$ of fabric [17] (E is the Young's modulus of fabric and L is the fabric thickness). This is due to the fact that the multi-filaments fabric does not have a mid-plane in bending, where its inside is compressed and outside is stretched.

Fabric strain energy (U_s) consists of stretching and shearing energies. This energy plays a pivotal role in the fabric deformation. The definition of U_s is given in polar coordinates [16]:

$$U_s = \frac{\pi EL}{1-\nu^2}\int_0^a \{\varepsilon_r^2 + \varepsilon_\theta^2 + 2\nu\varepsilon_r\varepsilon_\theta\} r dr \tag{7}$$

where ε_r, ε_θ are the radial and tangential normal strains. The relationships of strain and displacement are:

$$\varepsilon_r = \frac{du}{dr} + \frac{1}{2}\left(\frac{\partial w}{dr}\right)^2 \tag{8a}$$

$$\varepsilon_\theta = \frac{u}{r} \tag{8b}$$

By substitution of Eq. (8) into the preceding equation, the expression of U_s is obtained in the form:

$$U_s = \frac{\pi EL}{1-\nu^2}\int_0^a \{\left(\frac{du}{dr}\right)^2 + \frac{du}{dr}\left(\frac{dw}{dr}\right)^2 + \frac{u^2}{r^2} + \frac{2\nu u}{r}\frac{du}{dr} + \frac{\nu u}{r}\left(\frac{dw}{dr}\right)^2 + \frac{1}{4}\left(\frac{dw}{dr}\right)^4\} r dr \tag{9}$$

where the component $\left(\frac{\pi EL}{1-\nu^2}\int_0^a \left(\frac{2\nu u}{r}\frac{du}{dr} + \frac{\nu u}{r}\left(\frac{dw}{dr}\right)^2\right) r dr\right)$ represents the shearing energy and the rest is the stretching energy. Eq. (9) is a simplified expression due to the thin axis symmetrically deformed circular shape.

When a tight fabric sheet undergoes perpendicular loading, the work done (U_w) by the surface air pressure P per unit area from the initial to the equilibrium state is expressed as:

$$U_w = \iint_0^A Pw\, dxdy \tag{10}$$

As the circular fabric is deflected in the out-of–plane direction, the work done W caused by the air pressure can be obtained by integrating Pw across the area of the fabric based on Eq. (10):

$$U_w = 2\pi\int_0^a wPr dr \tag{11}$$

Therefore the total energy (U_T) for the clamped fabric deformation under an air pressure contains the bending energy (U_b), the strain energy (U_s) and the external work done (W):

$$U_T = U_b + U_s - U_w \tag{12}$$

Where '—' in Eq. (12) represents the external energy to the deformed fabric. In Eq. (12), U_b concerns with the fabric out-of-plane deformation; U_s concerns with the fabric in-plane deformation; U_w denotes the work done by the air pressure.

As to the assumed deflected fabric shape Eq. (4), the first order and the second order of derivatives with respect to the fabric radius (r) are:

$$\frac{du}{dr} = \frac{\pi\varphi}{a}\cos\frac{\pi r}{a} \tag{13a}$$

$$\frac{dw}{dr} = -\frac{\pi w'}{2a}\sin\frac{\pi r}{2a} \tag{13b}$$

$$\frac{d^2w}{dr^2} = -\frac{\pi^2 w'}{4a^2}\cos\frac{\pi r}{2a} \tag{13c}$$

By substituting Eq. (13) into Eq. (6) and Eq. (9), then integrating over the clamped fabric, and integrating Eq. (11), the results are:

$$U_s = \frac{\pi EL}{1-\nu^2}\left(\frac{\pi^2\varphi^2}{4} - \frac{\pi\varphi w'^2}{4a} - \frac{\varphi w'^2\pi^3}{32a} + \frac{\nu\varphi\pi w'^2}{3a} + \frac{\pi^2 w'^4}{64a^2} + \frac{3\pi^4 w'^4}{1024a^2} + \frac{\varphi^2}{2}\ln 2\right) \tag{14a}$$

$$U_b = \frac{\pi^3 D w'^2}{4a^2}\left(\frac{\nu\pi}{2a} + \ln\frac{\pi}{2}\right) \tag{14b}$$

$$U_w = 4\left(1 - \frac{2}{\pi}\right)Pw'a^2 \tag{14c}$$

In Eq. (14a), the condition $\frac{\partial U_s}{\partial\varphi} = 0$ that can make the U_s a minimum value:

$$\varphi = \pi w'^2\left(\frac{3-4\nu}{3a} + \frac{\pi^2}{8a}\right)/(2\pi^2 + 4\ln 2) \tag{15}$$

Inserting Eq. (15) and Eq. (14) into Eq. (12) with a numerical calculation:

$$U_T = \frac{0.52 + \nu - 0.3\nu^2}{1-\nu^2}\frac{ELw'^4}{a^2} + \frac{(2.83 + 3.87\nu)Dw'^2}{a^2} - 1.45Pw'a^2 \quad (16)$$

Then, application of the minimization, $\frac{\partial U_T}{\partial w'} = 0$, yields approximate expressions for the maximum displacement (w') and out-of-plane profile (w):

$$w' \cong a \cdot \sqrt[3]{\frac{1.45Pa}{EL} \cdot \frac{1-\nu^2}{2.08+4\nu-1.2\nu^2}} \quad (17a)$$

$$w = a \cdot \sqrt[3]{\frac{1.45Pa}{EL} \cdot \frac{1-\nu^2}{2.08+4\nu-1.2\nu^2}} \cdot \cos\left(\frac{\pi r}{2a}\right) \quad (17b)$$

Given an air pressure, Eq. (17) can predict the fabric maximum displacement and its deflected profile along a fabric diameter. The length of the deflected profile (l) is integrated across the fabric diameter as:

$$l = \int_{-a}^{a} \sqrt{1 + (f'(w))^2}\, dr \quad (-a \le r \le a) \quad (18)$$

where $f'(w)$ is the derivative of the function w (Eq. (17b)) to the variable r. All yarns are assumed with the same strain (ε) along their axes during the deformation. The average engineering strain (ε) of the deformed fabric is:

$$\varepsilon = \sqrt{\frac{s'}{s}} - 1 = \frac{l}{2a} - 1 \quad (19)$$

where s' is the surface area of the deformed fabric, and s is the area of the original fabric.

VERIFICATION

Two tight woven fabrics are employed to do experimental verification for w' and w across a diameter. Here, a novel experimental device is designed for the deformation verification.

Design of the Fabric Deformation Tester

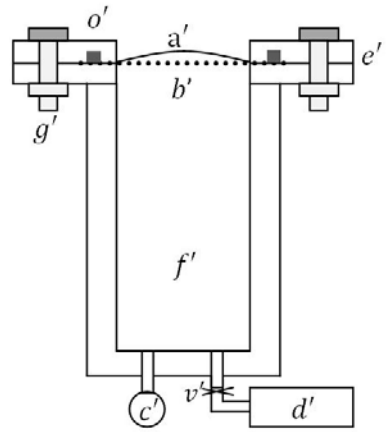

(a)

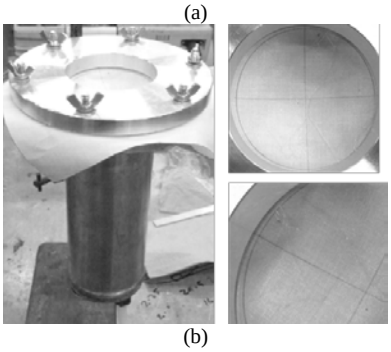

(b)

FIGURE 5. Fabric deflection tester: (a) construction sketch; (b) real tester and deformed fabric.

Figure 5a shows the design sketch of the fabric deformation tester. A stress-free flat circular fabric sheet (b') is clamped by two plates (e') with six bolts (g'), as shown in *Figure 5b*. The fabric edge is sealed by a compressed rubber ring (o') in plates. The testing diameter of the fabric in this device is 82 mm. A layer of cling film (a') is in place to ensure the system is airtight. The size of the film is slightly greater than that of the fabric to avoid influence on fabric deformation. The air in the container (f') is pumped by a vacuum pump (d'). There is a valve (v') that can control the vacuum level in the container. A vacuum pressure gauge (c') gives the pressure reading inside the sealed container. The device is designed to produce a vacuum pressure up to 1 *bar (=100 KPa)*.

A steel ball with diameter of 4 *mm* is used to determine the place of w'. A ruler is placed on the top plate across a diameter parallel to the fabric warp,

weft and 45° of warp/weft (bias) directions, respectively. A caliper is placed on the ruler perpendicularly and moved to determine the displacement of the deformed fabric. Each fabric deflection under a certain pressure load was repeated five times for the three directions with a fresh sample. Average fabric deflections for the repeats were given with standard deviations.

Experimental Materials

Two tight fabrics are listed in *Table I*. The fabric thickness (L) was determined using a FAST-1 device (Fabric Assurance by Simple Testing, CSIRO). A compaction pressure of 196 Pa was applied to the fabric during the measurement based on its test standard [21]. Fabric images were obtained using a ZEISS AxioScope A1 microscope. The images were used to measure the yarn spacing (distance between neighboring yarn centre lines), yarn width and yarn crimp angle (θ) by a free image analysis software Image-J [22]. The yarns in fabric A1 are made of multi-filaments without any twist. The yarns in fabric P2 are made of 65% PET and 35% cotton staple fibers subject to 'Z' spinning load with twist of 858/*m*. *Table I* show fabric A1 has overlapping yarns in weft direction and fabric P2 has very small pores between yarns, indicating their tight fabric structures.

TABLE I. Fabric specifications before air pressure loading (± SD).

Fabric	Composition and structure	L $10^{-3}\ m$	θ	D $10^{-6}\ Nm$	Yarn spacing $10^{-3}\ m$		Yarn width $10^{-3}\ m$	
					Warp	Weft	Warp	Weft
A1	100% Nylon filaments// plain weave	0.34 (±0.01)	70°	66.4	0.53 (±0.02)	0.45 (±0.01)	0.45 (±0.01)	0.52 (±0.01)
P2	PET65%/Cotton35% // plain weave	0.32 (±0.01)	76°	7.85	0.22 (±0.03)	0.33 (±0.01)	0.18 (±0.03)	0.20 (±0.03)

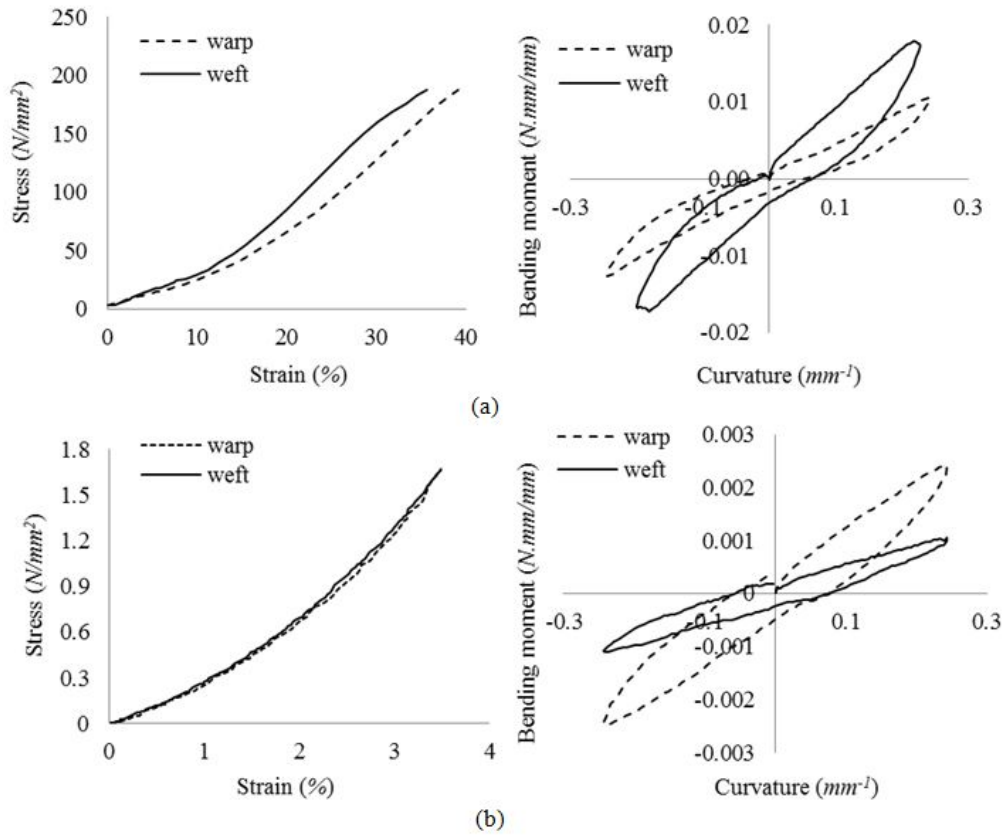

FIGURE 6. Tensile stress-strain and bending moment-curvature relationships of woven fabrics measured by KES: (a) fabric A1; (b) fabric P2.

Fabric Young's modulus (E) and flexural rigidity (D) were both measured by the KES system [23] at Unilever UK Central Resources. Two parameters were both tested using prepared samples with size $30cm \times 20cm$. In the KES tensile test, one side of fabric was gripped by two fixed grippers paralleled to its warp or weft yarns while the other side was gripped by movable grippers. If the movable grippers stretch a fabric forward with an increasing load up to 4.9 *N*, the increased tensile stress (*N/mm*) and fabric strain (%) was recorded. Its slope divided by the fabric thickness (assumed constant) was the fabric *E* value with a unit *Pa*. In the KES bending test, the movable grippers rotate around the fixed grippers with a fabric sample, a relationship of bending moment and fabric curvature was recorded as a closed curve. The slope of the first part of the curve is the D value with a unit Nmm.

Figure 6 shows the relationships of tensile stress-strain and bending moment-curvature for fabrics A1 and P2 obtained by KES. For fabric A1, the slope of tensile stress-strain is almost a constant when the strain is less than 10%. Then it shows nonlinearity as the strain increases. The slope keeps increasing for fabric P2. The initial average *E* values for warp and weft directions can be calculated as 247 *MPa* for fabric A1 and 148 *MPa* for fabric P2 by the slopes of curves. The movable grippers rotate clockwise from the original point. The slope of the first part of the curve in *Figure 6b* is the fabric D value. The expression $\frac{EL^3}{12(1-v^2)}$ was calculated as $889 \times 10^{-6}\ Nm$ for fabric A1 and $444 \times 10^{-6}\ Nm$ for fabric P2 based on the measured E and L with assumed the same Poisson's ratio (v) of 0.3 for both fabrics, which are much larger than the corresponding measured D values $66.4 \times 10^{-6}\ Nm$ of fabric A1 and $7.85 \times 10^{-6}\ Nm$ of fabric P2. This implies that the equation $D = \frac{EL^3}{12(1-v^2)}$ for calculating the bending rigidity of solid plates does not suit for textile fabrics. An attempt was made to measure the *v* values of the two tight fabrics using Digital Image Correlation (DIC) equipment according to Hursa's approach [11]. However, the results showed both to be larger than 1 which are not considered physically realistic. In the following section, a number of Poisson's ratios will be used to assess sensitivity.

RESULTS AND DISCUSSION

Maximum Displacement (*w'*)

The maximum displacement of tight woven fabric (w') was found to be at the centre of test area under the uniform air pressure. The prediction for w' is based on Eq. (17a), assuming three Poisson's ratio (v) values (0.2, 0.3 & 0.4) in the range of woven fabric [10, 11]. With a fixed v value, the predicted w' is proportional to the cubic root of the uniform air pressure (P) according to Eq. (17a). The comparisons of the w' values between the predictions ('*Pred*' curves) and experimental measurements ('*EXPT*' dots) are shown in *Figure 7*.

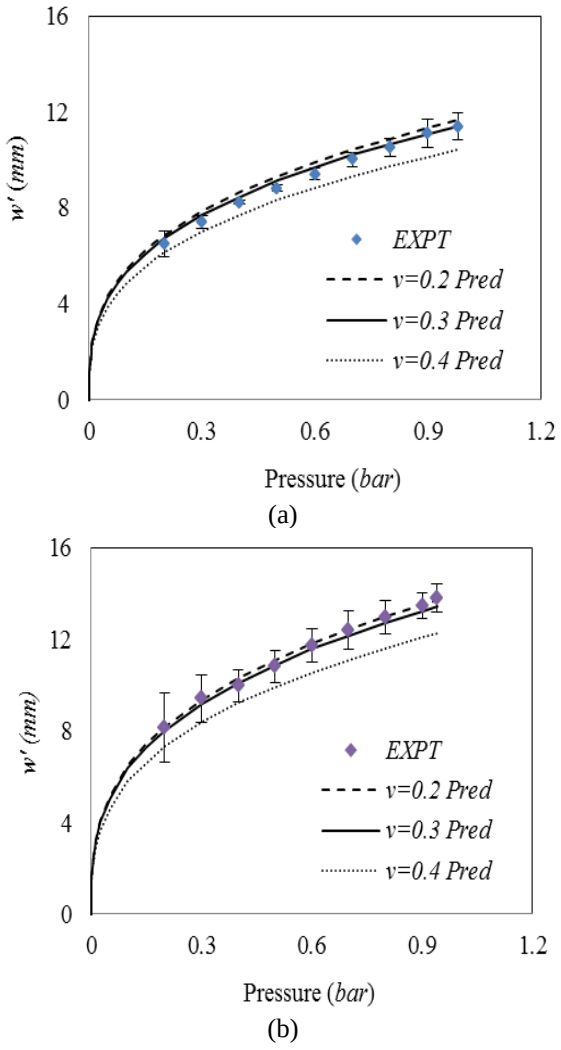

FIGURE 7. The maximum displacements under uniform air pressures of: (a) fabric A1; (b) fabric P2.

The experimental results in *Figure 7* show a nonlinear relationship of w' and P, which is close to the cubic root relationship in the prediction. The graphs also indicate that a smaller ν value can obtain a higher prediction of w', and the interval of the predicted curves between $\nu = 0.2$ and 0.3 is much less than that of 0.3 and 0.4, indicating that the relationship of w' and ν values is nonlinear, which can also be explained by Eq. (17a). The comparisons show that the ν value for fabric A1 is close to 0.3 while for fabric P2 is close to 0.2. In the graph, the w' value of fabric A1 is smaller than that of fabric P2 under the same air pressure. The reason is the smaller stiffness of fabric P2.

Deflection Profile (*w*)

Figure 8 compares the experimental measurements (‘*EXPT*’ dots) of the fabric deflection along a diameter with the corresponding predictions based on Eq.(17b) (‘*Pred*’ curves). Each ‘*EXPT*’ dot was the average measured values of three dots along three directions with the same distance to the sample test centre. The ‘*TexPred*’ profile in *Figure 8* is based on Eq. (1), which assumes the displacement equations are in polynomials. The fabric deflections in *Figure 8* are both under the same pressure of 1 bar. Here, the ν values for predictions are 0.3 for fabric A1 and 0.2 for fabric P2. The experimental results prove that the approximations Eq. (4) for the fabric deflections are reasonable and more accurate than that from Eq. (1).

The difference between the predictions from Eq. (1).and Eq. (4) is mainly displayed in the deflected profile near the fabric clamped edge. The prediction from Eq. (1).shows that the ‘vertical displacement’ declines slowly in this area due to the polynomial nature. The prediction from Eq. (4) shows a steep deflection profile in contrast due to the cosine function, which is also pointed out from the experimental image of *Figure 9.*

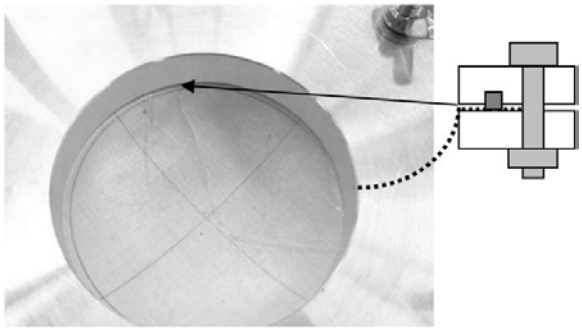

FIGURE 9. Deformation of fabric under uniform air pressure in experiment.

Figure 10 shows the deflected profiles of fabric A1 under different air pressures along the same fabric diameter. It is noted that the fabric is easier to be deformed under low air pressure, and a greater pressure achieves less increased displacement. This is due to the fabric interwoven structure compacted firstly under the air pressure, followed with the tension (loading) undertaken by the in-planar yarns. *Figure 10* can also be interpreted by the nature of Eq. (17a) for the cube root relationship of w' and P.

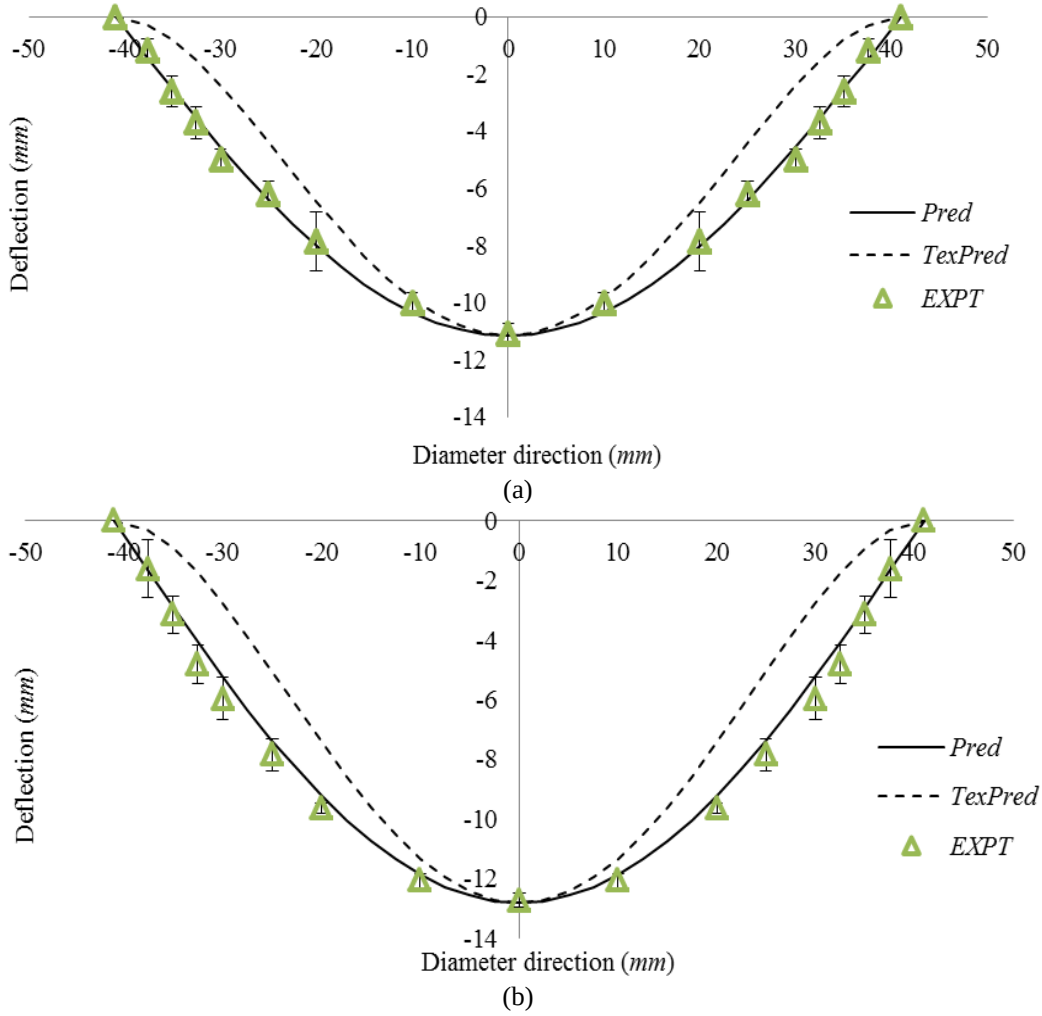

FIGURE 8. Comparison of experimental measurements against predictions of fabric deflection along a diameter: (a) fabric A1; (b) fabric P2 (Error bars represent standard derivation based on five repeats of tests at each point).

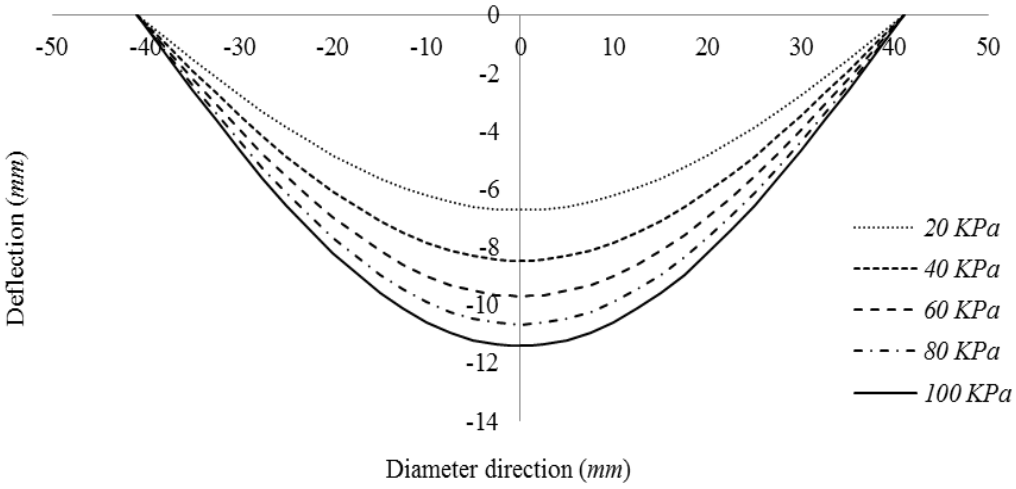

FIGURE 10. Deflection profiles of fabric A1 under different air pressures.

Factors Affecting the Fabric Deformation

Yarns are undulated with an inclined angle θ in a woven fabric as shown in *Figure 11*. The out-of-plane air pressure causes the yarn tensioning, leading to the crossover contact forces to shorten the effective distance of warp and weft yarns at yarn crossovers, increasing the inclined angle. The angle θ increases as the air pressure is increased as shown in *Figure 11*, which shows a schematic of the variation of half a yarn crimp under high air pressure. The original half length of the yarn crimp (S) and the inclined angle (θ) in a unit cell of woven fabric are increased to S' and θ', while the half fabric height $\frac{L}{2}$ is decreased to $\frac{L'}{2}$.

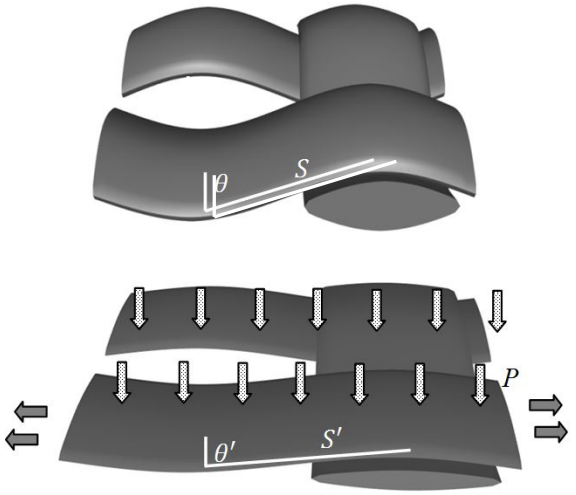

FIGURE 11. Schematic of the change of a unit cell cross-section under air pressure.

Based on Eq. (19) for the fabric strain under an air pressure, the increased inclined angle (θ') in the deformation can be calculated according to the trigonometric functions:

$$\cos\theta = \frac{L}{2S} \tag{20a}$$

$$\cos\theta' = \frac{L'}{2S(1+\varepsilon)} \tag{20b}$$

Therefore, the increased θ' is assumed simply as a function of ε and the original θ as follows:

$$\cos\theta' = \frac{\sin\theta}{(1+\varepsilon)^2} \tag{21}$$

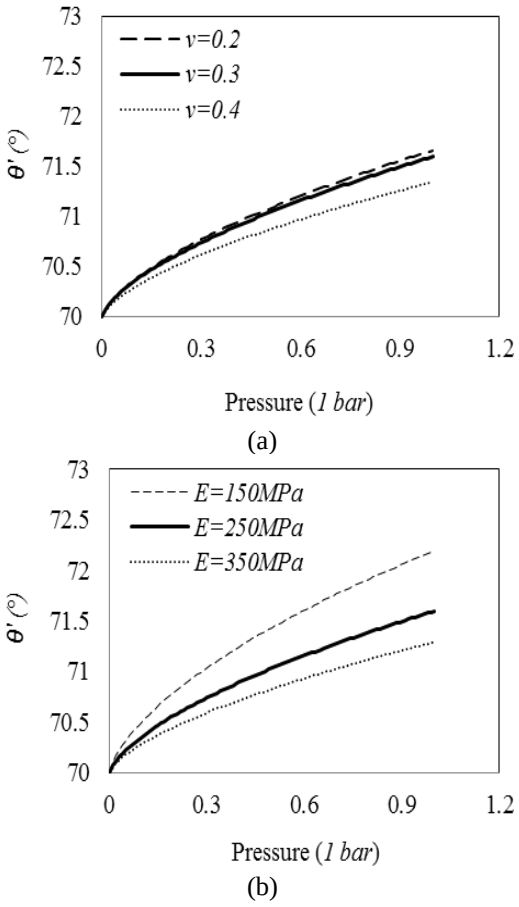

FIGURE 12. Effects of the air pressure on yarn inclined angle (fabric A1): (a) ν; (b) E

The relationship of the yarn inclined angle and air pressure can be found from Eq. (17), Eq. (18), Eq. (19) and Eq. (21). In fabric out-of-plane deformation, a larger ν value shows a relatively smaller variation of θ, as shown in the fabric A1 in *Figure 12a*. This can also be inferred from *Figure 7a*. The increased amount of θ at the beginning of pressure loading is much more than that from the subsequent stage. The reason is that the air pressure causes the yarn tensioning, which stretches the yarn interwoven structure and thereafter increases the yarn inclined angle and decreases the fabric thickness. The mean E values for both warp and weft directions are employed to predict the fabric out-of-plane deformation. *Figure 12b* shows that a larger θ' value is caused by a smaller E value under the same air pressure, as expected from the associated increase in the deflection.

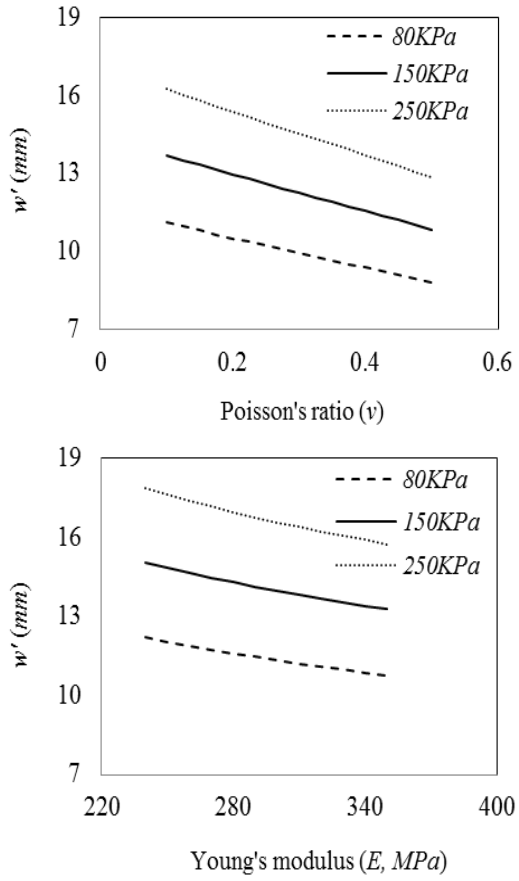

FIGURE 13. Effects of ν and E on the value of w' under different air pressures (fabric A1).

Figure 13 shows that the w' of fabric A1 is decreased with the increase of ν or E values. A larger ν means a smaller axial extension of the fabric with the same transverse strain; a greater E indicates the fabric is more difficult to deform. Thus, both factors reflect the effect on the decline curves of the maximum deflection.

CONCLUSION

An analytical model is proposed in this paper, for predicting the out-of-plane deformation of tight woven fabric under high air pressure. The key feature in the model development is that an energy-based approach is utilized for the equilibrium of the deformed fabric, which consists of bending energy, strain energy and work done by pressure. Minimization of the total fabric energy is used to derive the relationship of the maximum displacement (w') and the air pressure. The fabric deflection profile contains w' and a cosine function of the fabric radius.

A device based on vacuum pressure is designed to verify the fabric deformation model. Fabric w' and its deflection profile are determined experimentally. Deformations of two tight woven fabrics (an airbag fabric A1 and a cotton fabric P2) are compared between the analytical predictions and experimental measurements, showing their good agreements for both w' and deflection profile. Poisson's ratio can be approximately obtained from the w' prediction. The fabric deflection profiles are predicted based on the Poisson's ratios, showing relative good agreement with experimental data, especially at the clamped edge regions. A sensitivity study showed that an increase of either Young's modulus or Poisson's ratio can decreases the fabric out-of-plane deformation significantly.

REFERENCES

[1] Naik, N.K., Borade, S. V., Arya, H., Sailendra, M., Prabhu, S. V., *Experimental studies on impact behaviour of woven fabric composites: Effect of impact parameters.* Journal of Reinforced Plastics and Composites, 2002. 21(15): p. 1347-1362.

[2] Wielgosz, C., Thomas, J. C., *Deflections of inflatable fabric panels at high pressure.* Thin-Walled Structures, 2002. 40(6): p. 523-536.

[3] Clulow, E.E., Taylor, H. M., *An experimental and theoretical investigation of biaxial stress–strain relations in a plain-weave cloth.* Journal of the Textile Institute Transactions, 1963. 54(8): p. T323-T347.

[4] Kawabata, S., Niwa, M., Kawai, H., *Finite-deformation theory of plain-weave fabrics.1. shear-deformation theory.* Journal of the Textile Institute, 1973. 64(2): p. 62-85.

[5] Kawabata, S., Niwa, M., Kawai, H., *Finite-deformation theory of plain-weave fabrics.1. uniaxial-deformation theory.* Journal of the Textile Institute, 1973. 64(2): p. 47-61.

[6] Kawabata, S., Niwa, M., Kawai, H., *Finite-deformation theory of plain-weave fabrics.1. biaxial-deformation theory.* Journal of the Textile Institute, 1973. 64(1): p. 21-46.

[7] Taibi, E.H., Hammouche, A., Kifani, A., *Model of the tensile stress-strain behavior of fabrics.* Textile Research Journal, 2001. 71(7): p. 582-586.

[8] Freeston, W.D., Platt, M. M., Schoppee, M. M., *Mechanics of elastic performance of textile materials. 18. Stress-strain response of fabics under 2-dimensional loading.* Textile Research Journal, 1967. 37(11): p. 948-&.

[9] Boubaker, B.B., Assidi, M., Ganghoffer, J. F., *Evaluation of Poisson's ratio of textiles from mesoscopic models.* International Journal of Material Forming, 2010. 3(0): p. 81-84.
[10] Lu, Y., Dai, X., *Calculation of fabrics Poisson's ratio based on biaxial extension.* Journal of Textile Research, 2009. 30(9): p. 25-28.
[11] Hursa, A., Rolich, T., Razic, S. E., *Determining pseudo Poisson's ratio of woven fabric with a digital image correlation method.* Textile Research Journal, 2009. 79(17): p. 1588-1598.
[12] Wang, J., Paton, R., Page, J. R., *The draping of woven fabric preforms and prepregs for production of polymer composite components.* Composites Part A: Applied Science and Manufacturing, 1999. 30(6): p. 757-765.
[13] Sharma, S.B., Sutcliffe, M. P. F., *A simplified finite element model for draping of woven material.* Composites Part A: Applied Science and Manufacturing, 2004. 35(6): p. 637-643.
[14] Chang, S.H., Sutcliffe, M. P. F., Sharma, S. B., *Microscopic investigation of tow geometry changes in a woven prepreg material during draping and consolidation.* Composites Science and Technology, 2004. 64(10-11): p. 1701-1707.
[15] Hu, J.L., Chen, S. F., Teng, J. G., *Numerical drape behavior of circular fabric sheets over circular pedestals.* Textile Research Journal, 2000. 70(7): p. 593-603.
[16] Ugural, A.C., *Stresses in plates and shells (2nd edition).* second ed. 1999, Singapore: McGRAW-HILL International editions. 502.
[17] Lin, H., Clifford, M. J., Taylor, P. M., Long, A. C., *3D mathematical modelling for robotic pick up of textile composites.* Composites Part B: Engineering, 2009. 40(8): p. 705-713.
[18] Timoshenko, S., Woinowsky, K. S., *Theory of plates and shells (2nd Edition).* 1959, New York, London: McGraw-Hill Book Company, Inc. 580.
[19] Sagar, T.V., Potluri, P., Hearle, J. W. S., *Mesoscale modelling of interlaced fibre assemblies using energy method.* Computational Materials Science, 2003. 28(1): p. 49-62.
[20] Griefer, M.T., *Large deflection analysis using an energy method.* International Journal of Clothing Science and Technology, 2000. 12(4): p. 232-239.
[21] Boos, A.D., Tester, D. *SiroFAST Fabric Assurance by Simple Testing, A system for fabric objective measurement and its application in fabric and garment manufacture*. 1994; Available from: www.tft.csiro.au.
[22] *Image-J*. 2012 [cited 2012 17/05]; Available from: http://rsbweb.nih.gov/ij/features.html.
[23] Chan, C.K., Jiang, X. Y., Liew, K. L., Chan, L. K., Wong, W. K., Lau, M. P., *Evaluation of mechanical properties of uniform fabrics in garment manufacturing.* Journal of Materials Processing Technology, 2006. 174(1–3): p. 183-189.

AUTHORS' ADDRESES

Xueliang Xiao
Andrew Long
Hua Lin
Xuesen Zeng
The University of Nottingham
B02 Polymer Composites Group
ITRC Building
University Park
Nottingham, Nottinghamshire NG7 2RD
UNITED KINGDOM